ELSEVIER

Ceramics International 31 (2005) 1085–1090

CERAMICS INTERNATIONAL

www.elsevier.com/locate/ceramint

Improved direct bonding method of Nd:YVO_4 and YVO_4 laser crystals

Akira Sugiyama*, Yasunaga Nara

Advanced Photon Research Center, Kansai Research Establishment, Japan Atomic Energy Research Institute, 8-1 Umemidai, Kizu-cho, Souraku-gun, Kyoto 619-0215, Japan

Received 8 September 2004; received in revised form 12 October 2004; accepted 6 November 2004
Available online 1 February 2005

Abstract

We succeeded in the fabrication of bonded laser crystals composed of a neodymium-doped YVO_4 laser crystal (Nd:YVO_4) and its host crystals YVO_4 by a newly developed dry etching technique using an argon ion beam. The optical distortion caused by the bonded interface of size 5 mm × 6 mm was estimated to be 0.05λ at 633 nm. From the comparison of laser performance pumped by a laser diode, the bonded crystals could increase the laser output power by nearly twice that of the non-bonded crystals with the same degree of polarization of 99.2%. To analyze the mechanism of the enhanced reduction of the thermal load in the bonded crystals, numerical simulations with a finite-element method were also performed.

Keywords: Direct bonding; Laser crystal; Nd:YVO_4; Finite-element method

1. Introduction

Recent developments in laser diode arrays have resulted in high-power optical pumping of laser materials and contributed to the establishment of compact and high pulse repetition rate in solid-state laser systems. In the course of this trend, the improvement of heat transfer inside the laser materials is essential [1,2] and various methods of laser crystal bonding without the use of adhesive materials have been studied [3,4]. We have developed a direct bonding technique [5] using commercially available high quality laser crystals, and succeeded in bonding Ti:sapphire laser crystals [6–8]. In this method, the bonding surfaces of a stable oxide crystal were chemically processed to clean up and create a hydrophilic (–OH) thin layer for initial hydrogen bonding. However, to bond the different kinds of crystals, the chemical processes require the time consuming selection of suitable etchants and troublesome optimizations in the handling of the etching time and temperature. In most cases, hazardous strong acid and alkaline water are used in the chemical process. In addition, these etchants cannot be applied to hygroscopic and fluoride crystals.

To overcome these problems, a new dry etching process using argon ion beam irradiation instead of conventional chemical processes has been developed. As a specimen, we chose a Nd:YVO_4 laser crystal which has superior laser performance especially for industrial applications. It can be operated at a higher pulse repetition rate than that of the widely used Nd:YAG crystal [9]. However, the large absorbance of Nd:YVO_4 causes strong partial heating by continuous or highly repetitive optical pumping. In the worst-case scenario, the crystals are broken by thermal stress.

The purpose of this report is to describe our newly developed bonding technique and the results of the evaluation of the bonded crystals. We made interferometric measurements to estimate the bonded interface distortion. We also measured the laser performance of the output power and polarization to compare between bonded and normal single crystals. In the measurements, three types of

* Corresponding author. Tel.: +81 774 71 3365; fax: +81 774 71 3316.
E-mail address: sugiyama@apr.jaeri.go.jp (A. Sugiyama).

0272-8842/$30.00
doi:10.1016/j.ceramint.2004.11.009

Nd:YVO_4 laser crystal of different length were used. To study the advantage of the bonded crystal, we simulated the temperature and the thermal stress distributions inside the crystal by a finite-element method.

2. Experimental

The specimens were 1.1 at.% Nd:YVO_4 and non-doped YVO_4 crystals with a-cut surface dimension of 5 mm × 6 mm and 9 mm × 10 mm, respectively. The thicknesses of Nd:YVO_4 were 0.5, 1.0, and 3.0 mm. Each Nd:YVO_4 crystal was bound with two YVO_4 crystals with a thickness of 2 mm. Fig. 1 shows a schematic diagram of our procedure. The surfaces to be bonded were mechanically polished to a flatness better than 0.25λ at 633 nm. In the dry etching process, the polished surfaces were etched around 30 nm in depth by an argon ion beam for 50 min with an accelerating voltage of 200 V and a current of 10 mA. The specimens were placed in a clean atmospheric environment to create a natural hydrophilic layer on the surfaces. Hydrogen bonding was formed by applying a small pressure of around 0.1 MPa in the direction perpendicular to the contacted interface. The other side of the laser crystal was also contacted with a second YVO_4 in the same manner. In the next stage, the contacted specimen was treated in a high-temperature vacuum furnace to change the bonding formation from the hydrogen bonding to oxygen-bridged direct bonding by means of acceleration of the dehydration condensation, in which hydrogen bonding resulted in the reaction of OH + OH → H_2O + O. The heating at 873 K was maintained for 50 h in a vacuum of less than 3×10^{-3} Pa. This temperature can suppress opaque precipitation at the bonded interfaces [10,11]. Fig. 2 shows a photograph of the Nd:YVO_4 crystal bonded with non-doped YVO_4 ends. To evaluate the optical properties, we measured the transmitted wavefront by a Fizeau interferometer (Zygo: GPI-XPHR). The accuracy of the system is 0.01λ at 633 nm. We also

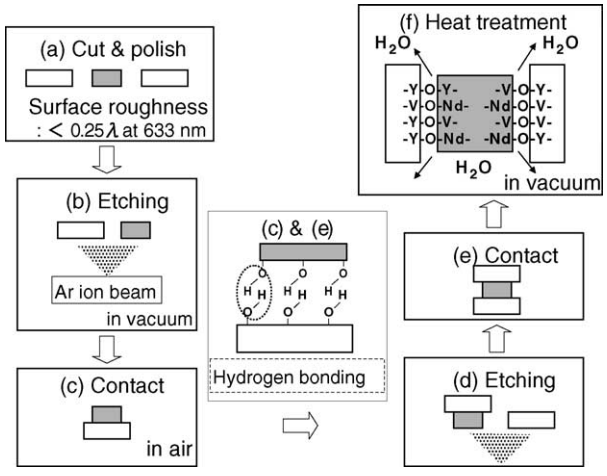

Fig. 1. Block diagram of the new direct bonding procedure using dry etching processes.

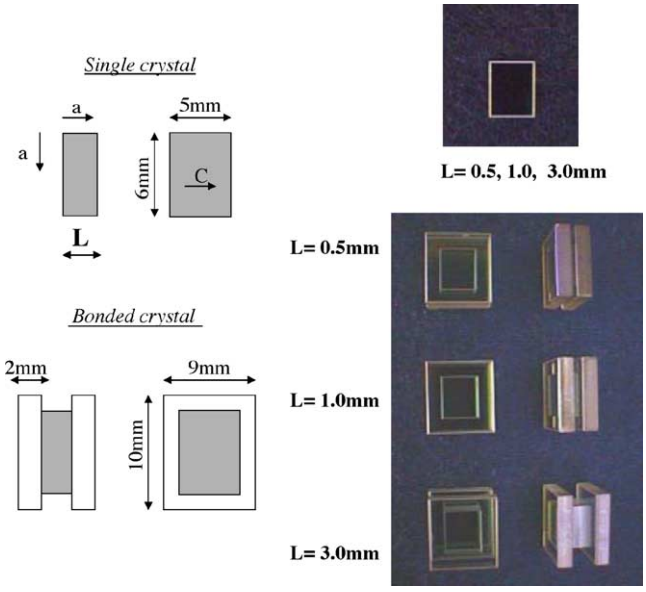

Fig. 2. Bonded laser crystals composed of Nd:YVO_4 and YVO_4 crystals. Three types with different laser crystal lengths were demonstrated. To discriminate the *c*-direction of the crystals, we bonded rectangular specimens.

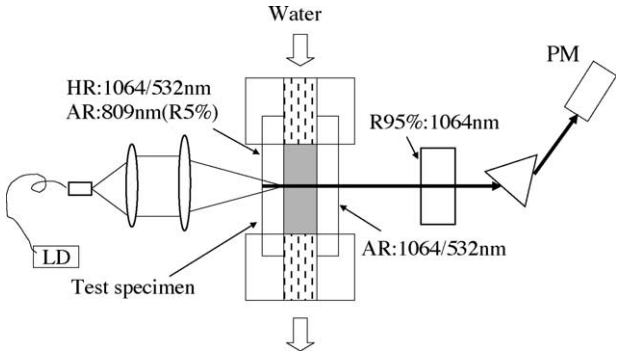

Fig. 3. Schematic diagram of the test bench for laser oscillation. PM is the power meter.

compared the output laser power and the degree of polarization between normal and bonded crystals using the same cavity length of 30 mm pumped by a fiber coupled CW laser diode array, schematically shown in Fig. 3. Each specimen was held in a copper block cooled by water with a temperature which was controlled to be 288 ± 1 K. In the measurements of the polarization pattern of the output beam, a Glan Taylor prism having an extinction ratio of 5×10^{-5} was used.

3. Results and discussion

The measured transmitted wavefront included three elements, i.e., crystal inhomogeneity, distortion by roughness of the polished surfaces, and distortion derived from the bonded interfaces. For the evaluation of inhomogeneity, we

Table 1
Optical distortions observed from transmitted wavefront measurements

	Crystals	Wavefront (*P–V*)
Inhomogeneity	YVO_4	0.007λ/mm
	Nd:YVO_4	0.010λ/mm
Wavefront distortion by polished surfaces		0.028λ

measured the wavefront for different lengths of the Nd:YVO_4 and YVO_4 crystals. The results are summarized in Table 1. The measured wavefront of a bonded crystal having 5 mm in total length was 0.116λ. As a result, the distortion of bonded interfaces was estimated to be 0.05λ.

Fig. 4 shows the measured polarization patterns. Single crystals were pumped with a low power of 4 W to reduce the thermal effect for the patterns. In contrast, the bonded crystals were pumped with a power of 20 W. The estimated degrees of polarization for the single and bonded crystals were 99.3% and 99.2%, respectively.

The comparison of laser output power is shown in Fig. 5. In Fig. 5(a), we cannot find a significant difference in both output curves till the pump power reaches 10 W. However, the normal crystal broke at over 10 W due to the strong thermal load. On the other hand, the bonded one kept increasing in the output power, then saturated at the pump power of around 16 W. In Fig. 5(b) and (c), the bonded crystals increased the output power in the same manner as (a).

To clarify the advantage of heat reduction in the bonded crystals, we constructed finite-element models and used thermo-analysis programs [12,13]. As YVO_4 has small anisotropy, a difference of 2.5%, in the thermal conductivity, we employed an isotropic model to reduce the calculation complexity. The equation of thermal conduction in the isotropic media can be written in the form [14],

$$Q = \rho C \frac{\partial T}{\partial \tau} - \mathrm{div}\,\kappa \cdot \mathrm{grad}\,T, \tag{1}$$

where ρ, C, T, τ, κ, Q are the density, the specific heat, the temperature, the heating duration, the thermal conductivity, and the calorific value per unit volume, respectively. On the assumption that the quantum efficiency of Nd:YVO_4 is 80%, the Q along the pump direction is given by the following equation,

$$Q(x) = -0.2 \times \frac{\mathrm{d}I}{\mathrm{d}x} = 0.2 \times \alpha I_0 \exp(-\alpha x), \tag{2}$$

where I_0 is the initial pumping laser flux at the incident optical surface and α is the averaged absorbance of the σ and π polarizations at the pump laser wavelength. In this calculation, we ignored the laser output power, and considered only the dominant pump power. The intrinsic thermal properties of Nd:YVO_4 and YVO_4 are assumed to be equal.

Fig. 6 shows the calculated results of the thermal distribution which appeared in the pumping condition of 10 W. When the thickness of the laser crystal was as little as 0.5 mm as shown in Fig. 6(a), a high-temperature area was distributed along the whole crystal length, because the length was too short to absorb the pump light completely. When the thickness became over 1.0 mm, the temperature of the right plane lowered, and an asymmetric temperature distribution appeared. In the bonded crystals, the distributions extended along the z-direction since the YVO_4 crystals acted as transparent radiators. The bonded crystals decreased the highest temperatures in all cases shown in Table 2.

In the normal single crystals, the heat transfer through the optical surfaces of size 5 mm × 6 mm are restricted since the surfaces are exposed to air that has a small thermal conductivity of around 1/200 of the YVO_4 crystal. The heat caused by optical pumping is mainly removed from the four crystal rim surfaces attached to the copper block. Therefore, the rate of heat reduction strongly depends on the thickness of the laser crystal. With a thicker single crystal, the cross section of the rim became wider. As a result, the hot spot temperature decreased. On the other hand, the hot spot temperatures of the bonded crystals showed less dependence on the thickness of the laser crystal since heat transfer through the bonded

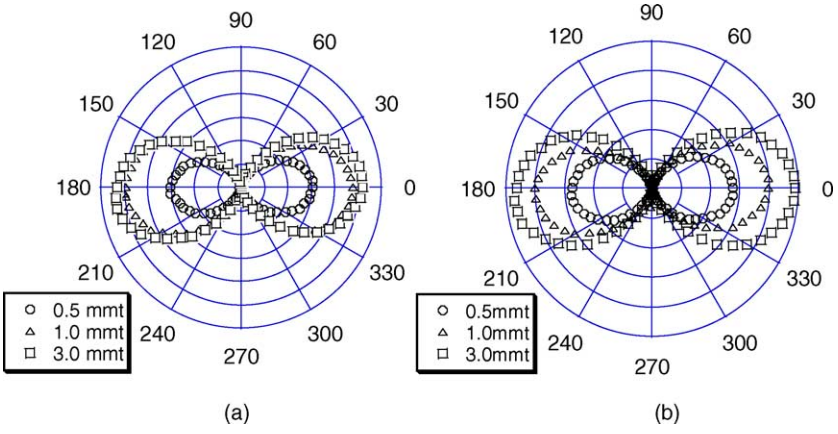

Fig. 4. Comparison of the polarization patterns. The normal single crystals (a) and the bonded crystals (b). 0–180° in these figures refers to the direction of E||C.

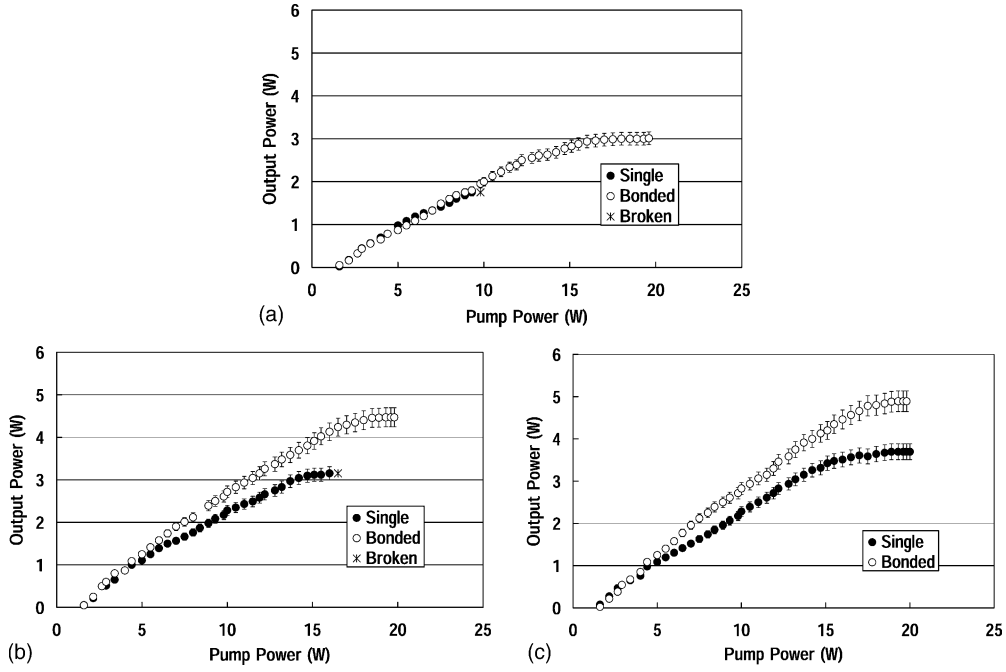

Fig. 5. Comparison of the Nd:YVO_4 laser outputs. The thicknesses of the laser crystal were 0.5 mm (a), 1.0 mm (b), and 3.0 mm (c).

interfaces was so efficient that the heat reduction via the host crystals became dominant. From the ratio of the gradients in the fitted equations for each maximum temperature shown in Table 2, it is concluded that the bonded crystals improved the cooling effect by about 1.6–2.3 times more than the normal single crystals.

In the evaluation of thermal stress depending on the temperature distribution inside the crystals, we calculated the values of the Von-Mises equivalent stress [15]. In Fig. 5(a) and (b), the normal single crystals broke at a pump power of around 10 and 16.5 W, respectively. With the fitted equations shown in Table 2, these thermal stresses are estimated to be 71.9 and 92.4 MPa.

To assess the reliability of these calculated data, we performed a fracture test of the YVO_4 crystals. When the concentrated load is placed on the center of the sample with

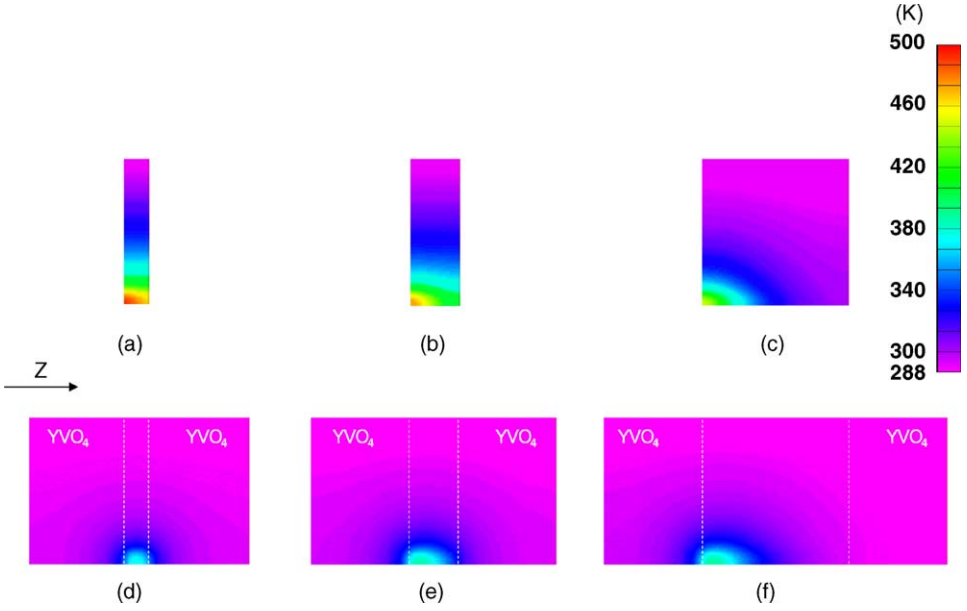

Fig. 6. Calculated temperature distributions. The arrow shows the pumping laser direction *Z*. The top row shows the normal single crystals. The thicknesses of the laser crystal are 0.5 mm (a), 1.0 mm (b), and 3.0 mm (c). The bottom row shows the bonded crystals. The broken lines indicate the bonded interfaces. The thicknesses of the laser crystal are 0.5 mm (d), 1.0 mm (e), and 3.0 mm (f).

Table 2
The value of highest temperature and the largest thermal stress calculated for different thicknesses of Nd:YVO_4

Nd:YVO_4 thickness	Pumping power (W)	Bonded		Single	
		Temperature (K)	Thermal stress (MPa)	Temperature (K)	Thermal stress (MPa)
0.5 mm	10	377.0	23.3	491.5	71.9
	20	466.6	46.8	695.5	148.5
Fitted equations		T (K) = 8.93P (W) + WT	S (MPa) = 2.35P (W)	T (K) = 20.37P (W) + WT	S (MPa) = 7.31P (W)
1.0 mm	10	389.7	30.8	476.9	54.8
	20	492.0	60.5	666.4	114.2
Fitted equations		T (K) = 10.20P (W) + WT	S (MPa) = 3.05P (W)	T (K) = 18.91P (W) + WT	S (MPa) = 5.60P (W)
3.0 mm	10	392.5	33.9	451.1	33.4
	20	497.0	70.3	614.9	71.5
Fitted equations		T (K) = 10.45P (W) + WT	S (MPa) = 3.45P (W)	T (K) = 16.35P (W) + WT	S (MPa) = 3.52P (W)

In the fitted equations, T, S, P, and WT are the highest temperature, the largest thermal stress, the pumping power, and the cooling water temperature, respectively.

a rectangular cross section of $b \times h$, the largest bending stress σ_{max} can be written in the form [16],

$$\sigma_{max} = \frac{3}{2}\frac{Wl}{b \times h^2}, \quad (3)$$

where W is the concentrated load and l is the length of the sample. In bending fracture measurements with specimens having 0.5 mm thickness, the crystals broke at a concentrated load of 1.2 ± 0.3 kgf. From the experiment, the largest bending stress was estimated as follows,

$$\sigma_{max} = 84.7 \pm 20\,\text{MPa} \quad (4)$$

Since the estimated thermal stresses of 71.9 and 92.4 MPa agree well with this experimental value of σ_{max}, we were assured that our calculation by the finite-element method is reliable.

Fig. 7 shows the calculated thermal stress distributions for the pumping condition of 10 W. For normal crystals, the largest stress appeared in the area of the highest temperature shown in Fig. 6. The hot area caused a parabolic expansion of the crystal in the surrounding air, which distributed the stress along the left plane of the crystal as shown in Fig. 7(c). On the other hand, the bonded crystals showed specific thermal stress profiles. The position of the largest stress was different from the position of the highest temperature. It shifted to the bonded interface. The largest compressed stress occurs between the hot spot area and the left hand portion of YVO_4 bonded crystal. Therefore, the durable bonding is essential for the interface in order to prevent thermal fracture, however, the maximum stress is decreased in comparison with the normal single crystals as shown in Table 2. From the ratio of gradients in the fitted equations,

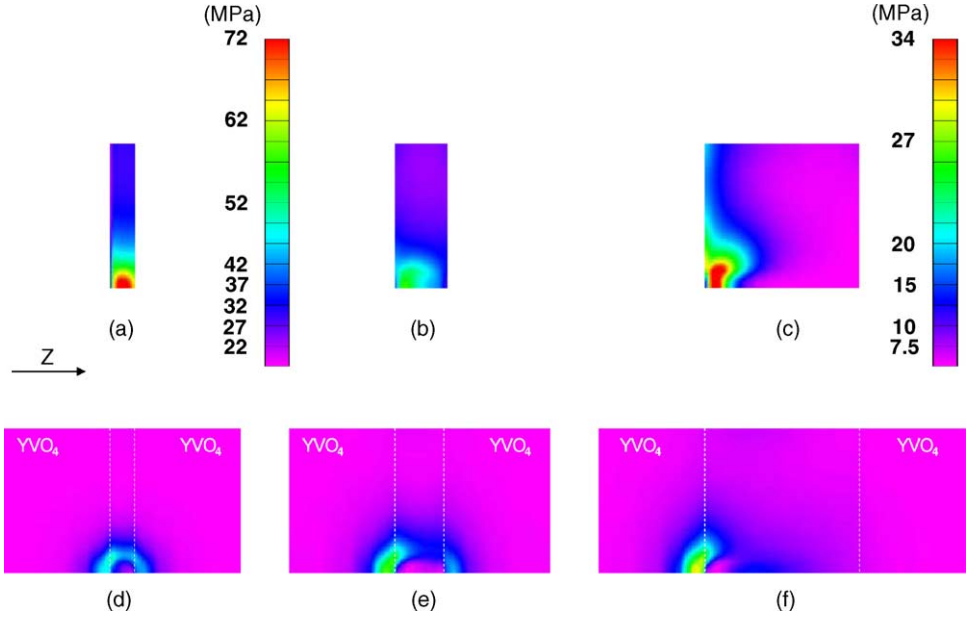

Fig. 7. Calculated thermal stress distributions. The results were calculated from the temperature distributions shown in Fig. 6. The color scale for (a) and (b) is shown in the middle of both figures. Another scale on the right side is for figures (c–f).

bonded crystals could improve the stress reduction at about 1.02–3.11 times that of normal single crystals.

4. Conclusions

Nd:YVO_4 and YVO_4 crystals were successfully bonded by our improved method using the dry etching process which can be applied to other crystals. Optical measurements proved that the bonded crystals had superior laser performance in the comparison with normal Nd:YVO_4 crystals. The cooling performance was analyzed by a finite-element method. The result showed that the temperature of the pumped surface was significantly reduced due to the predominant heat transfer through bonded interfaces. The calculated thermal stress based on the temperature distribution agreed well with the measured fracture limit of the crystal. The bonded crystal constructed by our method is applicable as a laser gain material for improving heat transfer in the case of high power optical pumping.

Acknowledgement

The authors thank M. Katsumata for his assistance in the bonding experiments.

References

[1] R. Weber, B. Neuenschwander, M. Mac Donald, M.B. Roos, H.P. Weber, Cooling schemes for longitudinally diode laser-pumped Nd:YAG rods, IEEE J. Quantum Electron. 34 (1998) 1046–1053.
[2] A. Nishimura, A. Sugiyama, T. Usami, K. Ohara, Improved cooling performance of ytterbium-doped glass combined with sapphire, J. Mater. Sci.: Mater. Electron. 14 (2003) 1–3.
[3] E.C. Honea, R.J. Beach, S.B. Sutton, J.A. Speth, S.C. Mitchell, J.A. Skidmore, M.A. Emanuel, S.A. Pane, 115-W Tm:YAG diode-pumped solid-state laser, IEEE J. Quantum Electron. 33 (1997) 1592–1600.
[4] M. Tsunekane, N. Taguchi, H. Inaba, Efficient 946-nm laser operation of a composite Nd:YAG rod with undoped ends, Appl. Opt. 37 (24) (1998) 5713–5719.
[5] M. Shimbo, K. Furukawa, K. Fukuda, K. Tanzawa, Silicon-to-silicon direct bonding method, J. Appl. Phys. 60 (8) (1986) 2987–2989.
[6] A. Sugiyama, H. Fukuyama, T. Sasuga, T. Arisawa, H. Takuma, Direct bonding of Ti:sapphire laser crystals, Appl. Opt. 37 (12) (1998) 2407–2410.
[7] A. Sugiyama, H. Fukuyama, Y. Kataoka, A. Nishimura, Y. Okada, Feasibility study of a direct bonding technique for laser crystals, Proc. SPIE 4231 (2000) 261–268.
[8] A. Sugiyama, H. Fukuyama, Y. Kataoka, Y. Okada, Evaluation of a bonded region in a direct bonded Ti:sapphire laser crystal, technical digest, CLEO/Pacific Rim 2001, WH3-3, 2001, pp. II 460–II 461.
[9] R.A. Fields, M. Birmbaum, C.L. Fincher, Highly efficient Nd:YVO_4 diode-laser end-pumped laser, Appl. Phys. Lett. 51 (23) (1987) 1885–1886.
[10] A. Sugiyama, H. Fukuyama, M. Katsumata, Y. Okada, Nd:YVO_4 and YVO_4 laser crystal integration by a direct bonding technique, Proc. SPIE 4944 (2002) 361–368.
[11] A. Sugiyama, Y. Nara, K. Wada, H. Fukuyama, Interfacial properties of a direct bonded Nd-doped YVO_4 and YVO_4 single crystal, J. Mater. Sci.: Mater. Electron. 15 (2004) 607–612.
[12] FEMAP, Structural Dynamic Research Corporation, 415 Eagleview Boulevard, Exton, PA 19341, USA.
[13] Photo-Thermo and Elas jω, Photon Co. Ltd., 7-27-1 Hikaridai, Seika-cho, Souraku-gun, Kyoto 619-0237, Japan.
[14] Wikipedia, The free encyclopedia, http://www.efunda.com/formulae/heat_transfer/conduction/Overview_cond.cfm#energy.
[15] M. Mizuno, Summery of the Material Mechanics, Yokendo, Tokyo, 1981, 68 pp. (in Japanese).
[16] T. Kunio, The Principles of the Solid Mechanics, Baifukan, Tokyo, 1977, 219 pp. (in Japanese).